ISSN : 0974 - 7494 Volume 8 Issue 8

Nano Science and Nano Technology
An Indian Journal

Full Paper

NSNTAIJ, 8(8), 2014 [312-319]

# Effect of annealing on optical and antimicrobial properties of zinc oxide nanoparticles

**P.P.Sharmila[1]*, S.Sagar[2], Nisha J.Tharayil[3]**
[1]Department of Physics, S.N College, Kollam, Kerala, (INDIA)
[2]Department of Physics, Government College for Women, Trivandrum, Kerala, (INDIA)
[3]Department of Physics, S.N College for Women, Kollam, Kerala, (INDIA)
E-mail : sharmilavishram@gmail.com

## ABSTRACT

Nano particles of Zinc Oxide has received much attention due to their unique antibacterial, antifungal, UV filtering, catalytic and photo-catalytic activities. The Nano particles of Zinc Oxide are synthesized through a simple and novel technique using aqueous solutions of metal acetate and carbonate. An organic templating agent (EDTA) is used in this work to prevent agglomeration. The carbonate precursor obtained is heated on the basis of TGA to obtain the metal Nano composite. The effects of different parameters on particle size and morphology of ZnO powders is optimized by ''one at a time'' method. Under optimum conditions, spongy shaped, uniformed and homogeneous nanostructured ZnO nano powders with particle size few nm are obtained. The structural characterization of the nano powders are done using the X-ray diffraction and electron microscopy techniques. The optical characterizations are done using UV-Vis spectroscopy, FTIR and photoluminescence studies. The effect of Zinc oxide nanoparticles on the growth of few common water pathogens are studied to explore its use as antibacterial agent to be used in water purification. To understand the mechanism of antibacterial activity and to confirm the role of reactive oxygen species the samples are annealed at different temperatures and the microbial activity is probed.


## KEYWORDS

Nano particles;
Chemical synthesis;
Biological applications;
Water purification.

## INTRODUCTION

Over the past few years, synthesis and functionalism of nano structures have attracted great interest due to their potential applications in all fields of science. Nano metal oxide particles especially have emerged as novel antimicrobial agents which can be used for the effective removal of pathogens from water. Moreover the antimicrobial properties of metal oxide nanoparticles is coming up as the current interest in the researchers due to the growing microbial resistances against metal ions, antibiotics and the development of resistant strains. The antimicrobial efficiency of metal oxide nanoparticles depends on the particle size, presence of light, composition of aqueous medium used in assay etc. In the present work antimicrobial activity of Zinc oxide

nanoparticles are explored since ZnO is a biocompatible and non-toxic substance. Zinc oxide has been a steady point of attraction for researchers over the decade due to its fascinating properties like wide band gap 3.37 eV and high excitation potential 60 eV. Its applications are numerous and include sensors, solar cells, chemical and biological sensors, ultra violet absorbers, transducers, catalyst, short wave length light emitting diodes and room temperature ultraviolet lasing diodes etc[1-3]. The ZnO nanostructures with different morphologies are widely being investigated nowadays because of their great potential for use in biosensors, bio-imaging, drug delivery and other biological applications[4-6]. They exhibit good antimicrobial activity against many pathogens[7,8].

In the present work a simple and economical procedure is used for synthesizing nano sized Zinc Oxide. The ZnO nanoparticles obtained were thermally treated at various temperatures. The influence of temperature on structural, textural, and morphological properties of the materials was studied by powder X-ray diffraction, infrared spectroscopy, scanning electron microscopy. Zinc oxide is generally regarded as a safe material and can be used to inhibit growth of food pathogens and water pathogens. In this study the microbial activity of Zinc oxide nanoparticles on few water pathogens are studied and its variation in the microbial activity with sintering temperature are also studied. The five common pathogens, namely Shigella flexneri (ATCC 2908), Vitrio Cholera (MTCC 3906), Escherichia Coli (ATCC 25922), Staphylococcus aureus (ATCC 9144) and Salmonella typhimurium (ATCC 23564), are chosen for this study.

## MATERIAL AND METHODS

The chemicals used for the synthesis of nanoparticles, namely Zinc acetate, Ammonium carbonate and EDTA were obtained from MERCK. The Bacteria cultures were obtained from Institute of Microbial Technology (IMTECH) Chandīgarh.

### Synthesis of nanoparticle

The Nano Zinc Oxide is prepared using 0.1 Molar solution of Zinc Acetate and 0.1 molar solution of Ammonium Carbonate which were dropped simultaneously and slowly at the rate of 10ml per hour into 0.01 molar solution of EDTA under constant stirring. The white carbonate precipitate obtained was separated from the reaction mixture and washed several times with alcohol and then with distilled water to remove impurities and traces of chemicals used. The wet precipitate was allowed to dry naturally and then thoroughly ground to obtain metal carbonate precursor in the form of fine powder. Upon heating the obtained metal carbonate, to the required temperature, it decomposes to form metal oxide. The thermo gravimetric analysis (TGA/DTA) of the carbonate precipitate (Figure 1a) showed a sudden weight lossat 400$^0$C to 450$^0$C indicating conversion from carbonate to oxide and hence the temperature of calcination was fixed at 500$^0$C. The TGA/DTA of the sample was taken using Perkin-Elmer diamond TGA/DTA apparatus.

The analysis was performed in the temperature range from 28$^0$C to 800$^0$C at a heating rate of 15$^0$C/min under nitrogen atmosphere. The atmosphere of calcination and the rate of increase of temperature etc., also

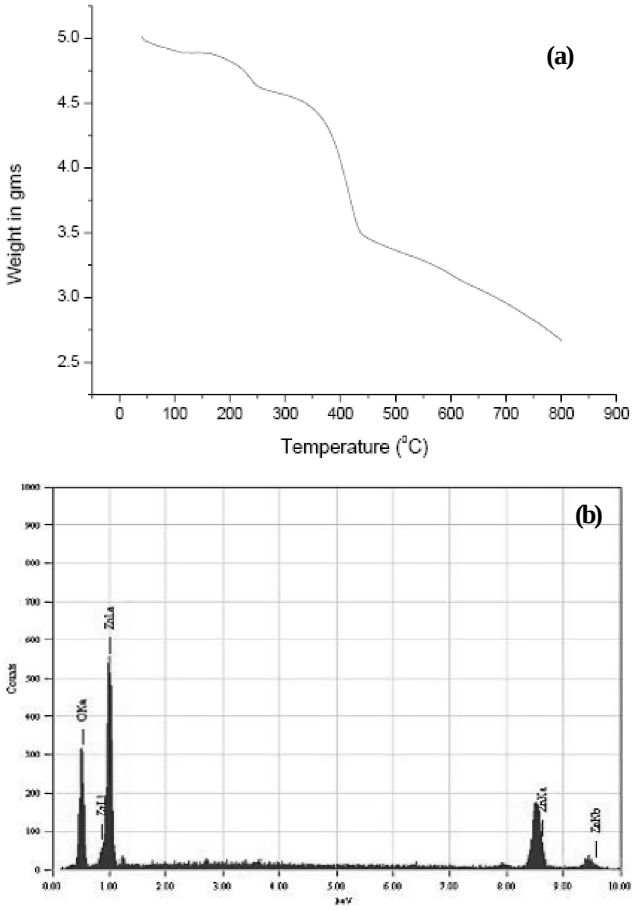


**Figure 1 : (a) TGA spectrum of carbonate precipitate, b) EDAX spectrum of as prepared sample (Z1)**

Full Paper

play an important role in the morphology and defect formation of nanoparticles. The carbonate precursor is transferred to a furnace at room temperature and then the temperature is increased slowly, at the rate of $5^0$/ minute, to $500^0$C. The duration of calcination was optimized to 3 hours on the basis of several observations done by varying the time.

The prepared samples were analysed using EDAX (Figure 1b) to check the presence of impurities if any and to have a correct knowledge about the chemical composition of the formed powder. The results of EDAX analysis (Figure 1b) shows that the powder is free from impurities and contains only Zinc and Oxygen. The samples synthesized were further heated in a furnace at temperatures $700^0$C and $900^0$C to study the effect of heating on the lattice, morphology and hence change in the bioactivity. Hereafter the samples annealed at temperatures $500^0$C, $700^0$C and $900^0$C will be referred as Z1,Z2, and Z3 respectively. The results of EDAX of the three samples namely Z1,Z2 and Z3 are given in TABLE 1. It shows the stoichiometry of the samples and composition

**TABLE 1 : Results of EDAX showing the composition of constituents elements in samples Z1, Z2 and Z3**

| Element | Mass% | | | Atom% | | |
|---|---|---|---|---|---|---|
| | Z1 | Z2 | Z3 | Z1 | Z2 | Z3 |
| O K | 18.24 | 7.42 | 5.22 | 47.68 | 24.66 | 18.37 |
| Zn L | 81.76 | 92.52 | 94.78 | 52.32 | 75.34 | 81.63 |
| Total | 100 | 100 | 100 | 100 | 100 | 100 |

## Bacterial studies

Filter paper disc diffusion technique was applied for determining anti-bacterial activity. Test organisms used to study microbial activity were collected from Institute of Microbial Technology, Microbial Type Culture Collection Centre, (IMTECH), and Chandigarh. The bacterial strains were maintained at $2\text{-}8^0$C on their respective medium. Muller Hinton Agar (MHA) medium used for bacterial culture was prepared and sterilized at $121^o$C for 15 minutes. After sterilization, required volume of the medium (20 ml) was poured into the sterile petri dishes and allowed to solidify. Pure culture is used as inoculum and 3-4 similar colonies were selected and transferred in to about 5 ml of Tryptone Soya Broth (TSB – Himedia M 1263). They were incubated at 37 °C for 8-12 hours till a light to moderate turbidity is developed. A sterile non-toxic swab on a wooden applicator dipped into the standardized inoculum was used for the application of inoculum to the agar plate. The entire agar surface of the plate was streaked with the swab three times, turning the plates at 60 angles between each streaking and allowed the inoculum to dry for 5-15 minutes with lid in place. The discs (Himedia sterile 6mm disc) impregnated with the sample, approximately 30 µl, using aseptic technique are then placed with centres at least 24mm apart. These plates are incubated immediately at 37°C and are examined after 16-18 hours or later. The zone showing complete inhibition is measured and the diameters of the zones to the nearest millimetre are recorded. Discs soaked in pure solvent, dimethyl sulfoxide (DMS) were used as control.

## RESULTS

### Structural characterisation

The XRD study was carried out using an 'X' pert pro model X-ray diffractometer employing Cu-K α radiation (make PAN analytical, Netherlands) at 40KV and 100mA at scanning rate of $8^0 min^{-1}$ from $2\theta = 10^0$ to $70^0$ from NIIST, Thiruvananthapuram. FTIR spectra of the sample were recorded in an FTIR Spectrophotometer (Thermo Nicolet, Avatar 370D). The SEM was recorded with a Hitachi- model S-3000H scanning microscope and TEM from National University, Singapore.

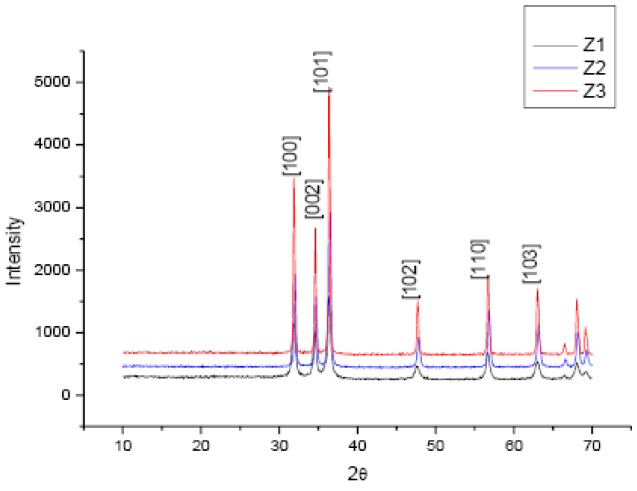


**Figure 2 : Xrd spectrum of samples**

## XRD analysis

The crystal structure of samples prepared were characterised through X-ray diffraction and the obtained pattern shows the formation of ZnO in wurzite structure. The X-ray diffraction spectrum of ZnO nanoparticles annealed at 500$^0$C,700$^0$C and 900$^0$C with prominent reflecting planes is shown in figure2. The peaks in the XRD spectrum corresponds to those from the JCPDS data (Powder diffraction File, Card No 079-0205), having hexagonal wurtzite structure with lattice constants a=b=3.241 A$^0$ and c=5.187 A$^0$. The lattice constants 'a' and 'c' of wurtzite structure of ZnO are calculated using relations (1) and (2) given below[9].

$$a = \sqrt{\frac{1}{3}}\frac{\lambda}{sin\theta} \quad (1)$$

$$c = \frac{\lambda}{\sin\theta} \quad (2)$$

Where λ is wavelength of X-ray used and θ Bragg's angle

It is clear from the XRD patterns of the three samples (Figure 2) that the FWHM decreases as the annealing temperature increases, which can be attributed to the grain growth that occurs at larger temperature. With an increase in oxidation temperature and duration of oxidation, the diffraction peaks become more intense and sharper, which indicates that the grain size became larger and the crystal quality has improved. The XRD peaks are broadened due to the nano crystalline nature of the particles. These nano-crystals have lesser lattice planes compared to the bulk, which contributes to the broadening of peaks in the diffractogram.

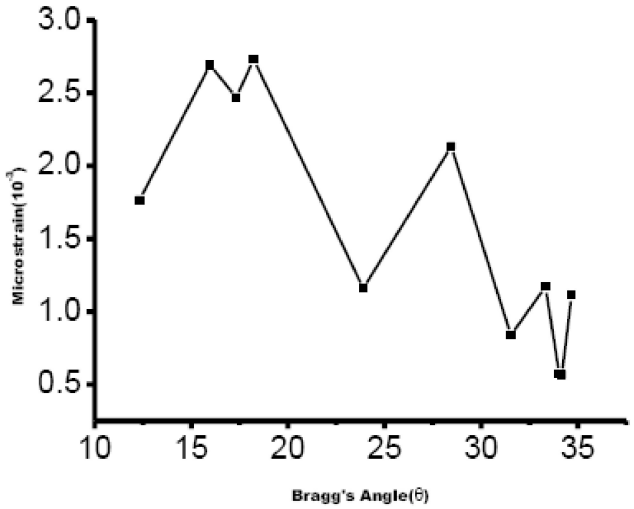


**Figure 3 : Microstrain vs Bragg's angle**

This broadening of the peaks could also arise due to micro strain of the crystal structures arising from defects like dislocations and twinning. These are believed to be associated with the nano crystals synthesized chemically as they grow spontaneously and the chemical ligands get less time to diffuse to an energetically favourable site The average crystallite sizes of the samples were calculated using Debye-Scherer equation (3) and microstrain 'e' using equation (4)

$$D = \frac{0.9\lambda}{\beta\ cos\theta} \quad (3)$$

$$e = \left(\frac{\lambda}{Dcos\ \theta} - \beta\right)\left(\frac{1}{\tan\theta}\right) \quad (4)$$

Here D is the crystallite size and β full width at half maximum of the peak with diffracting angle θ. The micro strain (e) for the sample Z1 is calculated using the equation (3) from data's obtained from XRD and is plotted against Bragg's angle (Figure 3).

**TABLE 2 : Parameters obtained from XRD of the three samples with particle size**

| Sample | hkl | D observed | D jcpds | Particle size (avg) | Lattice parameter | |
|---|---|---|---|---|---|---|
| | | | | | a | c |
| Z1 | 100 | 2.79845 | 2.8073 | 12.5±2.5 nm | 3.231372 | …….. |
| | 002 | 2.58872 | 2.5938 | | ……. | 5.17744 |
| | 101 | 2.46278 | 2.469 | | 3.230364 | 5.18491 |
| Z2 | 100 | 2.79502 | 2.8073 | 25±4 nm | 3.22741 | ….. |
| | 002 | 2.58661 | 2.5938 | | …….. | 5.17322 |
| | 101 | 2.46080 | 2.469 | | 3.230364 | 5.18491 |
| Z3 | 100 | 2.79968 | 2.8073 | 30±2.5nm | 3.232792 | …… |
| | 002 | 2.59004 | 2.5938 | | ….. | 5.18008 |
| | 101 | 2.46450 | 2.469 | | 3.235389 | 5.194369 |

## Morphological studies

The TEM spectrum (Figure 4) obtained shows that the particles are homogeneous, spherical in shape, and size falls in between 10-22 nm. The particle size distribution is also given as histogram.

The SEM pictures of the as prepared sample and annealed one (Z1, Z2 and Z3) are given in Figure 5. The micrographs show that nanoparticles are regular in size and shape and the annealed samples shows a good improvement in crystalline forms and the homogeneity

## Absorption studies

## UV-Visible spectroscopy

Absorption is a good probe of the overall band structure of a system because bands have a relatively

Full Paper

high density of states. PL emission on the other hand, tends to favour sparse low lying states because photo excited carriers rapidly thermalize through bands and closely spaced states. This feature makes it a suitable tool to analyse interface where defects and impurity levels are abundant. Using UV absorption spectrum (Figure 6) we get knowledge about band gap further evidence to quantum confinement

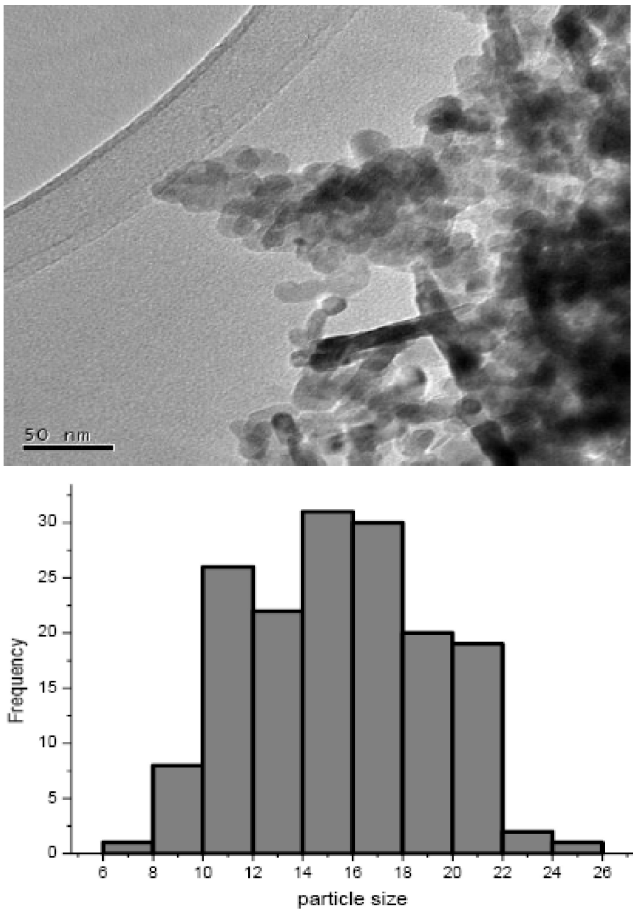


**Figure 4 : TEM of Zinc oxide nanoparticles and distribution of particle size**

The energy bands of the material is related to absorption coefficient α by the Tauc relation

$$\alpha h\nu = A(h\nu - E_g)^n \quad (3)$$

where A is a constant, hv is the photon energy and $E_g$ is the bandgap and n is an index which assumes values 1/2,3/2,2 or 3 depending on the nature of transitions responsible for absorption. Here the band gaps obtained from Tauc plots are 3.556eV (Figure 7), 3.342eV and 3.39eV respectively for sample Z1, Z 2 and Z3 all blue shifted from the bulk value of bandgap (3.3 eV)[10]. Brus had derived Effective mass approximation formula (EMA)[11] to explain the blue shift. The Effective mass approximation formula is given as

$$E_{eff} = E_g + \frac{h^2}{8\mu R^2} - \frac{1.8e^2}{4\pi\varepsilon\varepsilon_0 R} \quad (4)$$

Where $\frac{1}{\mu} = \frac{1}{me*} + \frac{1}{mh*}$, me* is the effective mass of electron (0.26 me), mh* is the effective mass of hole (0.59 me), R is the radius of the particle, ε is the dielectric constant at high frequency and $\varepsilon_0$ is the permittivity of free space. The second term in the equation is the quantum confinement for electrons and holes which lead to the blue shift[12] while third term is the coulomb energy term[13]. Due to the relatively small effective masses of ZnO, a bandgap enlargement is expected for particle radii less than about 8nm.

## FTIR analysis

The FTIR studies of samples were carried out in a Perkin-Elmer FTIR Spectrophotometer between 500 $cm^{-1}$ and 300$cm^{-1}$. The IR absorption spectra obtained is shown in Figure 7. The broad absorption band near 1600$cm^{-1}$ corresponds to carboxylate ions which dis-

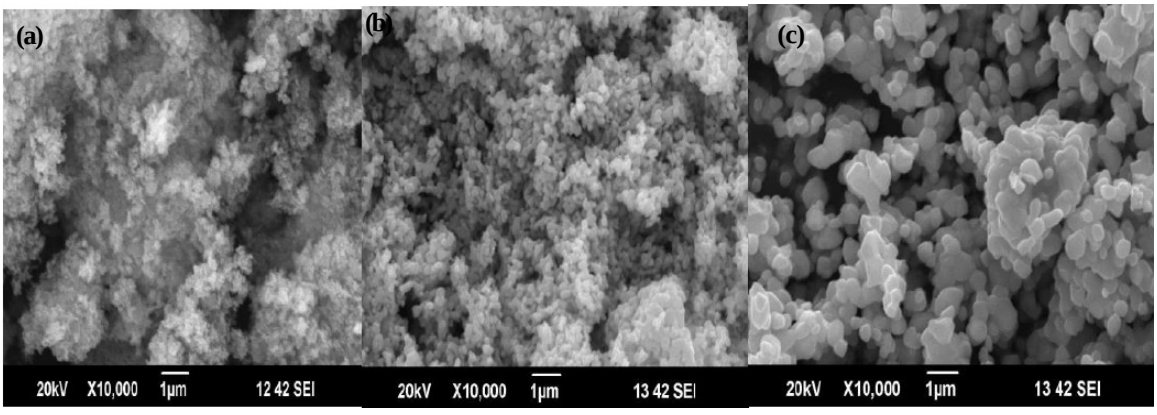


**Figure 5 : SEM micrographs of samples a) Z1, b) Z2, and c) Z3**

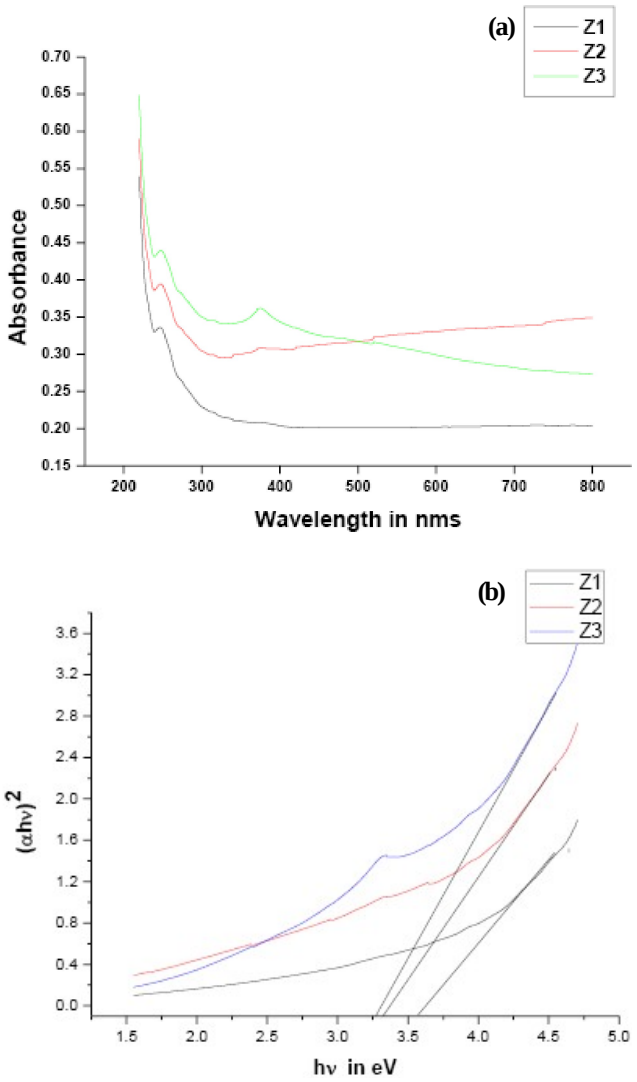


**Figure 6 : a) Absorption spectra of the samples. b) Tauc Plot showing variation in bandgap**

appeared in the sintered samples. The only other bands at 500-600 $cm^{-1}$ corresponds to bending and stretching modes of vibration of Zn-O bonds. Due to the nano size of the grains the IR active modes slightly shift due to the difference in coordination number and bond length but still the bands around 500 $cm^{-1}$ are typical of metal oxides. The broad band with low intensity at 3422 cm-1 in sample Z1 is related to vibration mode of (OH) group, indicating the presence of little amount of water adsorbed on the zinc oxide nanoparticles surfaces.

## Photo luminescence

The photoluminescence spectrum of ZnO corresponding to an excitation wavelength 250 nm is given in Figure 8. Room temperature PL spectrum (Figure 9) of the three samples show two prominent peaks, one intense sharp peak in the UV region centred at 323 nm with a small shoulder at 304 nm and another broad peak between 405-425 nm in the blue- green region. The UV emission at 323nm can be attributed to near band edge emission due to extinguishing of excitons. The other peaks in the blue green region, at 405-425 nm, is due to deep level or trap level emission formed due to the presence of oxygen vacancies in the nanoparticles synthesized. This results shows the presence of several defects in the lattice, like Zinc vacancies VZn, oxygen vacancies VO, interstitial Zinc ions Zni, antisites ZnO and transitions Zni→ VZn[3,10,18,19]. According to Chen et al, the green luminescence occurs as a result of electronic transitions from the ground and excited states of the shallow do-

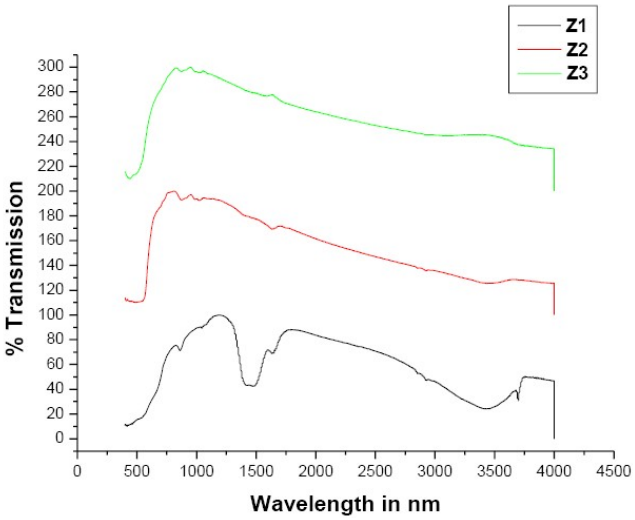


**Figure 7 : FTIR spectrum of the samples**

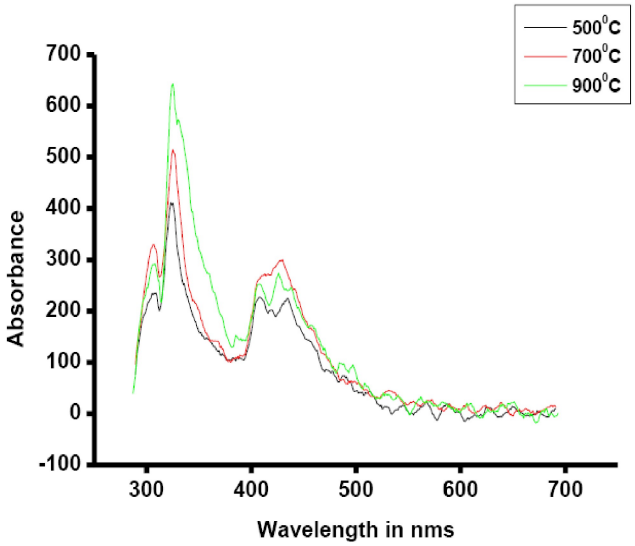


**Figure 8 : Photoluminescence spectra obtained for excitation wavelength 250 nm**

Full Paper

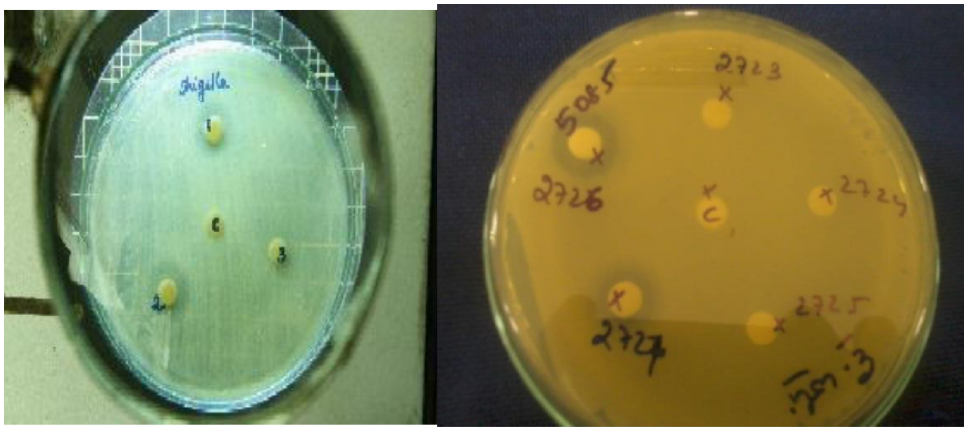


**Figure 9 : Photographs showing the inhibition Zones obtained for a) Shigella flexneri and b) E.Coli**

nor to the deep acceptor (VZn)[14]. Further Rodnyi et al suggest on the basis of data of fellow researchers that in zinc oxide with an excess of zinc (ZnO:Zn), oxygen vacancies VO, *F*-centers are responsible for green luminescence[15] which is in quite agreement with results obtained.

However the exact reason and a quantitative study to understand factors on which intensity of this emission depends is yet to be understood clearly, but many have attributed green emission to the strongly ionized oxygen vacancy and emission is resulted from the radiative recombination of photo generated hole with an electron occupying the oxygen vacancy.

## Bacterial studies

The antibacterial activity against five water pathogens namely Shigella flexneri, Salmonella Typhymuris, Escherichia Coli, Staphylococcus aureus and V. Cholera are analysed for the three samples Z1, Z2 and Z3 and results are given in mm in TABLE 3. Maximum activity was obtained for Shigella flexneri (Figure 9) and minimum for Vitrio Cholera.

To effectively detoxify noxious organic pollutants the semiconductor photo catalyst generally requires ultraviolet (UV) light as the excitant source; the reason is that UV energy is greater than the band gap of the semiconductor, and it will deduce the electron hole pairs generated when the semiconductor is illuminated by UV. The electrons subsequently react with O2 in the sample to form superoxide radicals, while the holes react with the surface OH groups to form OH radicals. These radicals attack the organic molecule, which is eventually oxidized to become $CO_2$, $H_2O$, and HCl, thus achieving an antibacterial effect. Similarly to titanium oxide[16], ZnO can absorb light (UV or visible) which induces a separation of charge, generating a hole ($h+$) in the valence band and an electron ($e–$) in the conduction band:

**ZnO + hυ→ *e*– + *h*+ (on the surface of ZnO particles)**

At the surface of the excited ZnO particle, the valence band holes abstract electrons from water and/or hydroxyl ions, generating hydroxyl radicals (OH). In addition, electrons can reduce O2 to produce the superoxide anion $O_2$[16]. The obtained OH and $O_2$ ion can induce lipid peroxidation in membranes, DNA damage due to strand breakage or oxidized nucleotides and oxidation of amino acids and protein catalytic centres[17]. Another possibility is destruction of organic material in a direct reaction with positively charged ZnO particles. It is observed that ZnO shows bactericidal properties in case of complete absence of light also. The results obtained in this study show that the antibacterial activity reduces with annealing temperature indicating that increase in oxygen deficiency may have led to this reduction in activity. This proves that reactive oxygen species is the reason for antimicrobial activity of Zinc oxide nanoparticles.

**TABLE 3 : Results obtained for the microbial activity of prepared samples**

| Parameters | Diameter of clear inhibition Zone in mm | | |
|---|---|---|---|
| | Sample Z1 | Sample Z2 | Sample Z3 |
| Salmonella typhymurium | 8 mm | 7 mm | NZ |
| Shigellaflexneri | 12 mm | 10 mm | NZ |
| Vibrio cholera | NZ | 7mm | NZ |
| Staphylococcus aureus | 8 | 7 | 7 |
| Escherichia Coli | 7 | 7 | 7 |

## CONCLUSIONS

The Nano sizes of the samples are confirmed by the band gap energy using the effective mass model. The TEM also showed particles of size less than 20 nanometres. The morphology and shape of the crystals improved on annealing. The photoluminescence spectrum proved the presence of lattice defects due to oxygen vacancies which was hinted from the micro strain calculations and the slight yellow nature of the sample. The bacterial studies show that Nano Zinc oxide can be used for the effective removal of water pathogens and can be used for water purification.. The particle size and hence increased surface area as well as reactive oxygen species on surface determine the extent of antibacterial activity.

## ACKNOWLEDGEMENTS

The first author acknowledges UGC for the financial assistance and NIST and STIC for providing facilities for the analysis.

## REFERENCES

**[1]** Yong-Seok Choi, Jang-Won Kang, Dae-Kue Hwang, Seong-Ju Park; IEEE Transactions on electron devices, **57(1)**, 26-41 **(2010)**.
**[2]** Abhinandan Makhal, Soumic Sarkar, Tanujjal Bora, Sunandana Baruah, Joydeep Dutta, A.K.Raychaudhari, Samir Kumar Pal; Nanotechnology, **21**, 265-703 **(2010)**.
**[3]** D.C.Look; Mat.Sci.Eng.B, **80**, 383 **(2001)**.
**[4]** R.Jalal, E.K.Goharshadi, M.Abareshia, Mmoosavi, A.Yousefi, P.Nancarrow; Materials Chemistry and Physics, **121**, 198-201 **(2010)**.
**[5]** N.Padmavathy, R.Vijayaraghavan; Sci.Tech.Adv. Matter, 9 **(2008)**.
**[6]** Gangadeep Singh, Eadaoin M.Joyce, James Beddow, Timothy J.Mason; Journal of Microbiology, Biotechnology and Food Sciences, **2**, 106-120 **(2012)**.
**[7]** Krishna R.Raghupathi, Ranjith T.Koodali, Adhar C.Manna; Langumuir, 4020-4028 **(2011)**.
**[8]** T.Jin, D.Sun, J.Y.Su, H.Zhang, H.J.Sue; J.Food Sci., **74**, 46-52 **(2009)**.
**[9]** C.Surynarayana, M.Grant Norton; X-Ray Diffraction A Practical Approach, Plenum Press Newyork and London, **(1998)**.
**[10]** H.Huang, S.Mao, H.Feick, H.Yan, Y.Wu, H.Kind, N.Tran, E.Weber, R.Ruso, P.Yang; Science, **292**, 1897 **(2001)**.
**[11]** L.E.Brus; J.Chem.Phys., **79**, 5566 **(1983)**.
**[12]** A.I.L.Efros, A.L.Efros; Sov.Phys.Semicond., **16**, 772 **(1982)**.
**[13]** L.E.Brus; J.Chem.Phys., **80**, 4403 **(1984)**.
**[14]** H.Chen, S.Gu, K.Tang et al.; J.Lumin., **131**, 1189 **(2011)**.
**[15]** P.A.Rodnyi, I.V.Khodyuk; Optics and Spectroscopy, **111(5)**, 776-785.
**[16]** L.Brunet, D.Y.Lyon, E.M.Hotze, P.J.J.Alvarez, M.Wiesner; Environ.Sci.Technol., **43**, 4355-4360 **(2009)**.
**[17]** E.Cabiscol, J.Tamarit, J.Ros; Int.Microbiol., **3**, 3-8 **(2000)**.
**[18]** U.Ozgur, Ya.I.Alivov, C.Liu, A.Teke, M.A.Reshchikov, S.Dogan, V.Avrutin, S.J.Cho, H.Morkoc; J.Appl.Phys., **98**, 041-301 **(2005)**.
**[19]** J.H.Choi, H.Tabata, T.Kawai; J.Cryst.Growth., **226**, 493 **(2001)**.